Parallel processing in immune networks

Elena Agliari [*], Adriano Barra [†], Andrea Galluzzi [‡],
Francesco Guerra [§], Francesco Moauro [¶]

Feb 1 2012

Abstract

In this paper we extend our previous investigations on systemic features of the immune system, based on a statistical mechanics approach. In particular, we recently introduced a mean-field spin-glass model for the interaction between helper cells and the effector branches (B and K cells) able to reproduce, as emerging properties, several collective phenomena shown in real immune networks (e.g. the connection between autoimmunity and lymphoproliferative disorders or the breakdown of immunosurveillance by diminishing the amount of helpers in the system). Here, we go beyond the previous fully-connected approximation by introducing dilution in the interactions between helpers and B clones, and show that this makes the former able to orchestrate parallel strategies to fight several pathogens simultaneously. This is an important step forward toward a comprehension of these systems since dilution, which is a biological requisite, results in multitasking capabilities. The latter are indeed the core of the immune system as always multiple attacks are present in a host.

1 Introduction

While the first half of the XIX century saw triumphal discoveries in physics, ranging from quantum mechanics and general relativity up to the discovery of chaos, the second half has been probably dragged by biology: Among its several fields of investigation, immunology (both theoretical and experimental) is currently one of the most intensive and promising. (Adaptive) Immune systems are networks of lymphocytes exchanging chemical signals and proteins as cytokines or antibodies. In a nutshell, the main constituents of the immune system are the effector branches (made of by B cells and Killer cells) and the Helper cells [1]. B cells produce antibodies and are grouped into clones: each cell belonging to a given clone produces the same antibody, while different clones produce different antibodies. When a pathogen, e.g. a virus, enters the body, the clone producing the best matching antibody undergoes clonal expansion and secretes the antibody able to chemically bind the pathogen hence (possibly) avoiding the propagation of the infection. If the virus has already infected a host cell, the latter is killed (e.g. via lysis) by Killer cells and order is restored. Actually, responses by effector branches can take place only if another signal (beyond the presence of the antigen) occurs. This signal is promoted by helpers which coordinate/modulate the response by exchanging with the effector branches both eliciting (e.g. the interleukin-4 cytokine) and suppressive messages (e.g. the interleukin-10 cytokine). Given the large amount of its constituents (e.g. the complete B-repertoire in humans is estimated to range in $10^8 - 10^{10}$ clones) and the interest in understanding global 'collective" features of the immune system thought of 'as a whole", scientists are becoming attracted towards the potentiality of statistical-mechanics approaches even in this branch of theoretical biology (see for instance [8, 9, 32, 38, 45]). However, a theoretical motivation for the use of canonical disordered statistical mechanics in biological world is not so obvious as biological systems are not isolated, and the blind application of the second law of thermodynamics locally may be debatable. One can argue a sort of "local-reductionism": despite within the host all networks (e.g. neural, endocrine, immune, etc) interact synergically, as a first approximation they can be considered independently (as in the approach paved in neural networks [5]) and the cells building the system retain only their peculiar function (as for instance firing/not-firing a spike in the neural scenario, or secreting/not-secreting antibodies for the B-cells in the present context). Furthermore, one may escape theoretical justification showing accordance with data and noticing that the Maxwell-Boltzmann

[*]Università di Parma, Dipartimento di Fisica, Italy and INFN Gruppo di Parma
[†]Sapienza Università di Roma, Dipartimento di Fisica, Italy and GNFM Gruppo di Roma
[‡]Sapienza Università di Roma, Dipartimento di Fisica, Italy
[§]Sapienza Università di Roma, Dipartimento di Fisica, Italy and INFN Sezione di Roma
[¶]Sapienza Università di Roma, Dipartimento di Fisica, Italy

distribution (at least for linear forces, namely quadratic Hamiltonians) coincides with the prediction of the maximum entropy models in statistical inference [34, 35], widely used for fitting procedure without paying attention to the whole scaffold offered by statistical mechanics.

With this premise we continue the investigation of a model introduced in [4] and meant to capture, as emergent features, some collective properties of the immune system. The model is based on spin-glasses [37] and their equivalence with information processing systems [17] as Bolzmann machines and Neural networks. More precisely, the interactions between helper cells and B-cells via cytokines (which are both eliciting or suppressive) is shown to give rise to an effective Hebbian structure among helpers alone, in which they are able to develop "strategies" to coordinate properly the effector branches [4]. Interestingly, bypassing the previous mean-field approximation, where each helper interacts with each B-clone, toward a description where each helper interacts only with a fraction of the available repertoire of B-cells, which is a biological must [1], makes the "cognitive capabilities" of the helpers able to manage parallel processing. This means that helpers succeed in performing multiple retrievals (i.e., strategies, instructions for the B-cells) at the same time, without falling into spurious states (i.e. errors) typical of the underlying glassy nature of neural networks. This is an important step forward toward a rationale understanding of the systemic properties of immune networks.

The paper is organized as follows. In section 2 we review the minimal, fully-connected model previously introduced in [4], while in Sec. 3 we explain how dilution is introduced and we scaffold the statistical-mechanics analysis, then, in Sec. 4 we study in details the parallel retrieval performed by the system and in Sec. 5 we give some insights in the numerical methods exploited; finally, Sec. 6 is left for discussions on results and on future perspectives.

2 The minimal model: features and limitations

In this section we briefly review the minimal model we introduced in [4] for the core of the immune system. As in the original model there is full symmetry between the two effector branches B and K, in the following we consider only the B-branch.

At equilibrium, when no external antigens are present and neglecting second order subtleties as auto-activation due to Jerne cascades [28, 40, 8] (see also Sec. 3.1), the system is built by H different helper clones and B different B-cell clones. Each B-cell clone, say the i^{th}, is associated to a degree of activation, referred to as b_i, which represents the extent of the clonal size with respect to a given equilibrium value. Setting, without loss of generality, the equilibrium value equal to zero for all clones $i \in (1, ..., B)$, we have that $b_i > 0$ ($b_i < 0$) means that the clone has expanded (shrunk). Due to fluctuations, memory effects and noise, overall the distribution of the clonal activations for the effector branches $P(b_i)$ is assumed as a central Gaussian $\mathcal{N}[0, 1]$, in agreement with experimental results [36].

Interactions among B-cells (which are not treated here) exist too and, roughly speaking, work through a complementary affinity exchange such that if a B-cell (belonging to a clonal lineage) produces the antibody 10000 in some epitopal alphabet (see for instance the phase shape of [42, 43] or the interaction matrix of [8, 9]), its antibody can be recognized by the cells (clonal lineage) producing the anti-antibody 01111 or very similar variants. As a consequence, cells belonging to the same clone do not interact directly and there is no intra-clonal cooperative response to an external stimulus such as an antigenic attack. This would lead to a Michaelis-Menten [50][27] behavior of the B-cell response. On the other hand, the overall bell-shaped response [1] is the result of extra-clonal cooperative interactions and of interactions with helper cells (through cytokines).

As for helpers, the situation is quite different because they interact each others via cytokine signalling [36, 49] which is non-specific, so that intra-clonal response can be highly cooperative[2]. Thus, the activity h_i can be better approximated by a step function (a steep hyperbolic tangent), which can be seen as a digital switch w.r.t the B kinetics. Consequently, we define their status (active/inactive) as a binary Ising spin such that if $h_i = -1$ the i^{th} clone is quiescent, while if $h_i = +1$ it is firing, namely secreting cytokines[3].

[1] The reason is that the interaction between B cells and helper cells is essentially local: on the one hand B cells act on helpers as antigen presenting cells and this requires MHC-II:antigen to bind properly with the TCR available from the helper ensemble, on the other hand, helper cells act on B cells via cytokine exchanges which are diffusive and short-ranged

[2] In particular biochemistries quantify the property of cooperation by a direct measure of the Hill coefficient C [27][21], such that for its high values, e.g. $C \geq 4$ there is a strong sigmoidal shape in the response: The system shows unresponsiveness to small stimuli while it is maximally responding once the stimulus reaches a threshold and stay stable beyond.

[3] We stress that, as simplifying assumptions, we neglected details about the subclasses T_{h_1}, T_{h_2} [36] which would clarify the cytokine loops inside helpers and we neglected further the "hierarchical" strength of various cytokines [33] (e.g. interferons usually induce stronger responses w.r.t. interleukins) assuming all the chemical signals as equivalent and loosing a more complex alphabet for chemical messengers.

As cytokines may have either positive (expansion) and negative (suppression) signs, we model the system of B and H interactions as a bipartite spin glass admitting the Hamiltonian representation[4]

$$\mathcal{H}(h,b;\xi) = \frac{1}{\sqrt{H}} \sum_{i,\mu}^{H,B} \xi_i^\mu h_i b_\mu, \tag{1}$$

where ξ_i^μ is the cytokine connecting the i^{th} helper clone with the μ^{th} B-clone [5]. Hence, overall, $H \times B$ cytokines have to be defined.

The partition function $Z_{H,B}(\beta)$ of this system can be written as

$$\begin{aligned} Z_{H,B}(\beta) &= \sum_{\{h\}}^{2^H} \int \prod_{\mu=1}^{B} db_\mu e^{-\sum_{\mu=1}^{B} \frac{b_\mu^2}{2}} e^{\frac{\beta}{\sqrt{H}} \sum_{i\mu}^{HB} \xi_i^\mu h_i b_\mu} \\ &= \sum_{\{h\}}^{2^H} \exp\left(\frac{\beta^2}{2H} \sum_{ij}^{H} \sum_{\mu=1}^{B} \xi_i^\mu \xi_j^\mu h_i h_j \right) = \sum_{\{h\}}^{2^H} \exp[-\beta^2 \tilde{\mathcal{H}}(h;\xi)]. \end{aligned} \tag{2}$$

The parameter β^2 (in the following rescaled into β) rules the level of noise in the network, while the ratio $\alpha = \lim_{H\to\infty} B/H$ accounts for the difference in clonal sizes between helpers and B-cells, in the limit of large sizes.

Interestingly, the complex interactions between helpers and B-cells are absorbed, via marginalization, within a two-body Hamiltonian $\tilde{\mathcal{H}}(h;\xi)$, which turns out to be equivalent to the Hamiltonian of the Hopfield model which functions as an associative memory [5]. Here, neurons are replaced by helper lymphocytes and the memorized "patterns of information" correspond to particular strategies, encoded by cytokine secretions, for the B-cells. In the following we will refer to the generic element i as lymphocyte, spin or neuron, indifferently.

As well known from neural network theory [5], this system may show cooperative cognitive features only if $\alpha \leq \alpha_c$, where $\alpha_c < 1$ is a critical value implicitly offering the first global constraint for a correct performance of the immune system: Helpers must be more than B-cells; this is indeed confirmed experimentally [1].

Let us now see how the system responds to an external stimulus in the adiabatic limit. For simplicity we consider the case where all clones are made to expand; this peculiar situation actually corresponds to a real disease, known as Autoimmune Lymphoproliferative Syndrome (see for instance [47]). Therefore, in the partition function $Z_{H,B}(\alpha,\beta)$, we substitute the centered Gaussian weight $\exp(-\sum_\mu b_\mu^2/2)$ with $\exp[-\sum_\mu (b_\mu - b_0)^2/2]$, b_0 being the new reference value of clonal expansion. It is immediate to check [4] that when the bipartite spin-glass system is mapped into the neural network counterpart, a new term appears in the resulting (pseudo)-Hamiltonian $\tilde{\mathcal{H}}(h;\xi)$:

$$\beta\tilde{\mathcal{H}}(h;\xi) = \frac{\beta}{2H} \sum_{ij}^{H} (\sum_{\mu=1}^{B} \xi_i^\mu \xi_j^\mu) h_i h_j + \sqrt{\alpha\beta} b_0 \sum_{i}^{H} \eta_i h_i, \tag{3}$$

with $\eta \in \mathcal{N}[0,1]$. Thus, a clonal expansion, which can be thought of as ordered work, implies a production of "heat", thought of as a random field (a noise source), which affects helpers performance[6]. As a consequence, too strong responses (lymphocytosis) can be coupled with (transitive) autoimmune manifestations because the random fields prevail over retrieval; this offers a simple theoretical explanation to a common fact.

Therefore, the tunable parameters of the system are β, α and b_0; according to their mutual values the system described by $\tilde{H}(h;\xi)$ exhibits different behaviors (see Fig. 1). In the neural scenario, one can outline a region in the parameter space where the system is able to retrieve a given learnt bit-string

[4]Note that this Hamiltonian shares the same mathematical structure of the cost functions of the Boltzmann learning machine [14], whose thermodynamical equivalence with neural networks has been deepened in [10].

[5]The interaction between a B cell and a T cell is rather complex as it requires first that B-cells present, through their major histocompatibility complex, a peptide processed from the antigen previously detected, and this that must bind enough to the corresponding TCR of the helper [1]. Then, T-cells secretes cytokines directed to B cells themselves. While biologists distinguish between "helper" T-cells (secreting stimulatory cytokines) and "regulators" or "suppressors" to T-cells (secreting inhibitory cytokines), here we simply refer to helper cells. Indeed, the experimental research on details of these interactions is still ongoing. Along the same line, we adopt symmetric distributions for cytokines with a spirit close to the neural network counterpart [5]. The framework depicted is therefore meant to describe the behavior of the system after the antigen presentation by B cells, but prior to the possible, consequent clonal expansion.

[6]Note that the noise level β appears linearly in the "bulk" term, while under the square root in the noise term, mapping standard propagation of information in the former and random diffusion in the latter.

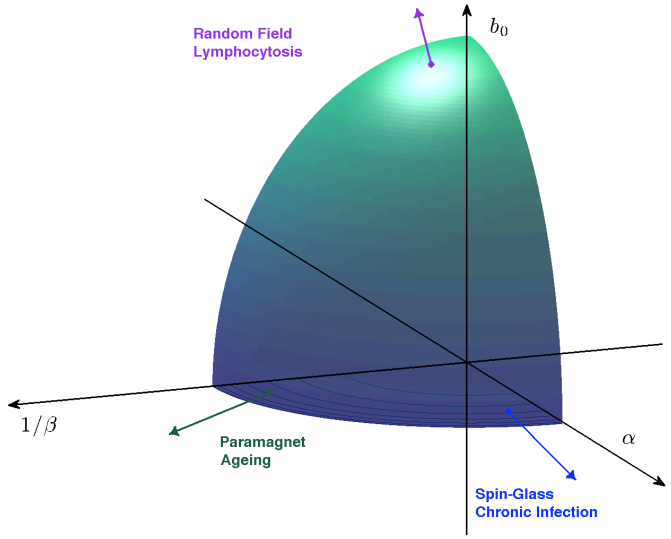

Figure 1: Schematic representation of the working (retrieval) region. The three normal ways to escape have been depicted: Random Field (too large or too low mean activity), Spin-Glass (too large relative number of patterns) and Paramagnetic (too large degree of noise). Such states correspond to unhealthy situations, namely lymphocytosis, chronic infections and senescence, respectively. The working region is restricted, by definition, to the quadrant $\alpha > 0$, $\beta > 0$.

of information, which corresponds to a particular pattern ξ^μ. How does this concept translate, in the immunological context?
This can be understood by introducing the B Mattis magnetizations $m_\mu = \frac{1}{H}\sum_i^H \xi_i^\mu h_i$, one for each B-clone. If, for example, the pattern of cytokine activation $\mu = 1$ has been retrieved, then $m_1 = 1$, which means that all helper states are parallel to the corresponding cytokines linking them to the first B-clone. As a consequence, all the inhibitor signals are absent while all the eliciting signals are present, namely, the assembly of helpers orchestrates the response against the antigen coupled to the first B-clone conferring to the latter the maximal strength for the clonal expansion. We stress that the Hamiltonian (3) shows gauge invariance (breakable with an external field [5], usually thought of as a threshold for firing in neural counterpart), which is lost in the bi-layered B-H network. In other words, the marginalizations performed in Eqs. (2) and (11) break the symmetry $h_i \to -h_i$. In fact, the H-H network is left invariant under the transformation $h_i \to -h_i$ for all $i \in (1, ..., H)$, while in the B-H network, having fixed the cytokine pattern, the same transformation leads to a change in the field felt by the connected B clones.

We finally underline that, within a pure fully-connected approach, each helper clone interacts with the whole B-repertoire, and the assembly for deciding about one single B-clone includes the whole helper ensemble, which are both unrealistic fatures given the huge sizes of such populations and the fact that interactions are essentially local and of diffusive nature. In what follows we remove the hypothesis of a fully-connected by-layered spin-glass network and we allow only a (small) fraction of the whole ensemble of helpers to coordinate the response of a given B-clone. As we will show, the resulting associative network made by helpers is able to parallel process, namely to manage several B-clones together at the same time, which is an emergent property much closer to the biological reality.

3 Getting closer to biology: Dilution in the B-H interactions

3.1 The refined model and its robustness

The purposes of this section is to generalize the original model in two ways.

First, we show that, even including intra-clonal cooperativity among B-cells (hence for dichotomic variables $b_i = \pm 1$) we can still retain, under a suitable expansion, a resulting helper network working as an associative working memory. This extension allows to incorporate even second order effects of clonal interactions in the B-repertoire previously neglected. For instance, a virus, e.g. represented by the string of information 0111, yields the clonal expansion of the lineage of B-cells producing the antibody 1000, and this, in turn, will drive the clonal expansion of the lineage of the B-cells producing the anti-antibody

0111; the latter, resembling (for receptor binding) the original virus, could elicit further the expansion of the clone 1000, resulting as a second-order cooperative feedback by the cells within the original clone. Therefore, the Gaussian variables for B-cells are replaced by dichotomic ones and we assume here that both H lymphocytes h_i and B lymphocytes b_μ take discrete values ± 1, where -1 stands for quiescence while $+1$ for a firing state (secretion of cytokines -for the H- or secretion of antibodies -for the B-); in particular, B clones are subjected to the following probability distribution:

$$P(b_\mu) = P\delta_{(b_\mu - 1)} + (1-P)\delta_{(b_\mu + 1)}, \tag{4}$$

where δ_x is the Kronocker delta function and $P \in [0,1]$, such that for values of $P \neq 1/2$, it acts as a bias mimicking the original b_0 parameter.

Then, we show how, by properly diluting the bipartite spin-glass by-layer of B and H cells, the associative helper network becomes able to handle parallel recall of several different patterns (strategies). We introduce the Hamiltonian of this new by-layer in complete analogy with the previous section as

$$\mathcal{H}(h,b;\xi) = -\frac{1}{\sqrt{H}} \sum_{\mu=1}^{B} \sum_{i=1}^{H} \xi_i^\mu b_\mu h_i. \tag{5}$$

When dilution is absent, free energy minimization shows that this Hamiltonian, for orthogonal patterns $\vec{\xi}^\mu \cdot \vec{\xi}^\nu = H \cdot \delta(\mu - \nu)$ (which results from uncorrelated distributions in the thermodynamic limit $H \to \infty$), tends to expand the μ^{th} B-clone (i.e. $m_\mu > 0$), but it provides the other clones with no net information (i.e. $m_{\nu \neq \mu} = 0$). Conversely, real immune systems are able to address a wide variety of antigens simultaneously managing several clones at the same time and, in this sense, we refer to parallel processing capabilities of the network. This property can be restated as the ability to have equilibrium states with several Mattis magnetizations different from zero, or above the noise level at finite volume, without being spurious states [5].

We introduce dilution in the couplings, by writing:

$$\xi_{i\mu} = \varepsilon_{i\mu} \cdot c_{i\mu}, \tag{6}$$

where $\varepsilon_{i\mu}$ assumes values ± 1, representing the excitatory or inhibitory quality of the link (cytokine), and $c_{i\mu}$ assumes values 1 or 0 representing, respectively, existence (1) or absence (0) of the link. Their probability distribution are:

$$P(c_{i\mu}) = d\,\delta_{(c_{i\mu})} + (1-d)\delta_{(c_{i\mu}+1)}, \tag{7}$$

$$P(\varepsilon_{i\mu}) = \frac{1}{2}\delta_{(\varepsilon_{i\mu}-1)} + \frac{1}{2}\delta_{(\varepsilon_{i\mu}+1)}, \tag{8}$$

where d can range continuously in $[0,1]$, allowing some intensive tuning[7]. Hence, we get the following distribution for $\xi_{i\mu}$:

$$P(\xi_i^\mu) = P(c_{i\mu}\varepsilon_{i\mu}) = \frac{(1-d)}{2}\delta_{(\xi_i^\mu - 1)} + \frac{(1-d)}{2}\delta_{(\xi_i^\mu + 1)} + d\delta_{\xi_i^\mu}, \tag{9}$$

such that for $d \to 1$ no network exists, while for $d \to 0$ the Hopfield model is recovered.

We can now proceed to the calculation of the partition function $Z_{H,B}(\alpha, \beta, d)$:

$$Z_{H,B}(\beta, d) = \sum_{\{h\}}^{2^H} \sum_{\{b\}}^{2^B} \exp[-\beta \mathcal{H}(h,b;\xi)]. \tag{10}$$

Summing the partition function over the b_μ distribution (Eq. (4)) we get

$$\begin{aligned} Z_{H,B}(\beta, d) &= \sum_{\{h\}}^{2^H} \prod_{\mu=1}^{B} \left[2P \cosh\left(\frac{\beta}{\sqrt{H}} \sum_{i=1}^{H} h_i \xi_i^\mu \right) + \exp\left(-\frac{\beta}{\sqrt{H}} \sum_{i=1}^{H} h_i \xi_i^\mu \right) \right] \\ &= \sum_{\{h\}}^{2^H} \prod_{\mu=1}^{B} \exp\left\{ \ln\left[2P \sinh\left(\frac{\beta}{\sqrt{H}} \sum_{i=1}^{H} h_i \xi_i^\mu \right) + \exp\left(-\frac{\beta}{\sqrt{H}} \sum_{i=1}^{H} h_i \xi_i^\mu \right) \right] \right\}. \end{aligned} \tag{11}$$

[7]We stress that the assumption of symmetry for cytokine distribution (see Eq. (8)) can be easily relaxed leading to a network with low level of activation and whose properties strongly resemble the standard ones [6].

Expanding, in the last line in Eq.(11), the logarithm of the hyperbolic sine at the second order we get

$$Z_{H,B}(\beta,d)=\sum_{\{h\}}^{2^H}\prod_{\mu=1}^{B}\exp\left\{(2P-1)\frac{\beta}{\sqrt{H}}\sum_{i=1}^{H}h_i\xi_i^\mu+[1-(2P-1)^2]\frac{\beta^2}{2H}\sum_{i,j}^{H}h_ih_j\xi_i^\mu\xi_j^\mu\right\}. \tag{12}$$

We can split the contribution of the field φ_i insisting on the generic h_i lymphocyte in two terms: $\varphi_i = \varphi_i^{ext}+\varphi^{int}$:

$$\varphi_i^{ext}\equiv(2P-1)\frac{\beta}{\sqrt{H}}\sum_{\mu}^{B}\xi_i^\mu,\quad \varphi^{int}\equiv[1-(2P-1)^2]\frac{\beta^2}{2H}\sum_{j}^{H}\sum_{\mu}^{B}\xi_i^\mu\xi_j^\mu h_j.$$

The latter results from the effective two-body interactions among helpers and preserves the Hebbian structure necessary for the retrieval. Conversely, the former, for sufficiently large B, by the central limit theorem (CLT), approaches a Gaussian variable and can be thought of as a term of noise. Hence, posing $\eta=\mathcal{N}[0,1]$, we can write

$$\sum_{\mu=1}^{B}\xi_i^\mu=\eta_i\sqrt{B\,(1-d)}. \tag{13}$$

Shifting β^2 to β to rescale noise we get

$$\beta\tilde{\mathcal{H}}(h;\xi,\eta)=-[1-(2P-1)^2]\frac{\beta}{2H}\sum_{i,j}^{H}h_ih_j\sum_{\mu}^{B}\xi_i^\mu\xi_j^\mu-(2P-1)\sqrt{\frac{\beta B\,(1-d)}{H}}\sum_{i=1}^{H}h_i\eta_i, \tag{14}$$

where the first and the second terms mirror, respectively, the associative network and the perturbing random field (due to poly-clonal activation) of Eq. (3). Assuming for simplicity $P=1/2$ so to start studying the system in the absence of external stimuli, we get the effective Hamiltonian

$$\tilde{\mathcal{H}}(h;\xi)=-\frac{1}{2H}\sum_{i,j}^{H}J_{ij}h_ih_j=-\frac{1}{2H}\sum_{i,j}^{H}\sum_{\mu}^{B}\xi_i^\mu\xi_j^\mu h_ih_j, \tag{15}$$

whose properties will be investigated in the rest of the paper.

3.2 Notes about the coupling distribution

As it is immediate to check, each missing link between the i^{th} helper cell and the μ^{th} B-cell in the bipartite B-H network appears as a 0 (i.e. $\xi_i^\mu=0$) in the i^{th} entry of the bit-string ξ^μ in the equivalent associative network, which ultimately affects the interaction matrix $\mathbf{J}=J_{ij}$. Of course, the larger the degree of dilution, the stronger the difference between such (random) coupling matrix and its Hopfield counterpart. This section is devoted to the investigation of the properties of the matrix $\mathbf{J}$.

Let us consider a set of H nodes labeled as $i=1,...,H$ and let us associate to each node a string of length B and built from the alphabet $\{-1,0,1\}$, meaning that the generic element ξ_i^μ, with $i\in[1,H]$ and $\mu\in[1,B]$, can equal either ±1 or 0. For the H-H network described by the Hamiltonian in Eq. (15), the interaction strength between two arbitrary nodes i and j is given by

$$J_{ij}=\sum_{\mu=1}^{B}\xi_i^\mu\xi_j^\mu. \tag{16}$$

Of course $J_{ij}\in[-B,B]$. Equation (16) gives rise to a network of mutually and symmetrically interacting nodes, where a link between nodes i and j is drawn whenever they do interact directly ($J_{ij}\neq0$), either imitatively ($J_{ij}>0$) or anti-imitatively ($J_{ij}<0$).

First, one can calculate the probability that two nodes (since they are arbitrary we will drop the indexes) in the H-H network are linked together, namely

$$P_{\text{link}}(d,B)=P(J\neq0;d,B)=1-P(J=0;d,B)=1-\sum_{k=0}^{B}P_{\text{sum}-0}(k;d,B), \tag{17}$$

where $P_{\text{sum}-0}(k;d,B)$ is the probability that two strings display (an even number) k of non-null matchings summing up to zero; otherwise stated, there exist exactly k values of μ such that $\xi_i^\mu\xi_j^\mu\neq0$ and they are

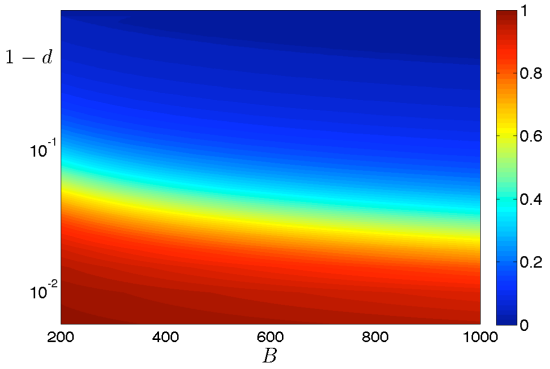

Figure 2: (Color on line) Contour plot for $P(J=0;d,B)$ representing the probability that the coupling between two arbitrary nodes is zero, as a function of B (linear scale) and d (logarithmic scale).

half positive and half negative. In particular, $P_{\mathrm{sum}-0}(0;d,B)=[d(2-d)]^B$, because this is the probability that, for any $\mu\in[1,B]$, at least one entry (either ξ_i^μ or ξ_j^μ or both) is equal to zero. More generally,

$$P_{\mathrm{sum}-0}(k;d,B)=\left(\frac{1-d}{2}\right)^{2k}[d(2-d)]^{B-k}\binom{B}{k}\left[2^k\binom{k}{k/2}\right], \tag{18}$$

where the first and the second factors in the r.h.s. require that k entries are non-zero and the remaining $B-k$ entries are zero; the third factor accounts for permutation between zero and non-zero entries, while the last term is the number of configurations leading to a null sum for non-null entries. Therefore, we have

$$P(J=0;d,B)=[d(2-d)]^B\sum_{k=0}^{B}\left[\frac{(1-d)^2}{2d(2-d)}\right]^k\binom{B}{k}\binom{k}{k/2}, \tag{19}$$

whose contour is shown in Fig. 2. As for its asymptotic behavior, we distinguish the following cases (for simplicity we assume B finite and even):

$$P(J=0;d,B) = 1-B(1-d)^2+\frac{3}{4}B(B-1)(1-d)^4+\mathcal{O}(1-d)^6 \tag{20}$$

$$P(J=0;d,B) = \frac{(-1)^{B/2}\sqrt{\pi}}{\Gamma(1/2-B)\Gamma(1+B/2)}(1-2B\,d)+\mathcal{O}(d^2)\approx\frac{1-2B\,d}{4^{B/2}}\binom{B}{B/2}+\mathcal{O}(d^2). \tag{21}$$

The average number of nearest neighbors per node $\langle z\rangle_{d,B,H}$ follows immediately as $\langle z\rangle_{d,B,H}=HP_{\mathrm{link}}(d,B)$.

More generally, we can derive the coupling distribution $P(J;d,B)$, once having defined $P_{+1}(k)$, $P_{-1}(k)$ and $P_0(k)$, as the probability that, given two strings, they display k matches each equal to $+1$, -1 and 0, respectively, namely

$$P_{+1}(k;d)=P_{-1}(k;d)=\left[\frac{(1-d)^2}{2}\right]^k,\quad P_0(k;d)=[d(2-d)]^k. \tag{22}$$

Hence, we can write

$$\begin{aligned}P(J;d,B) &= \sum_{l=0}^{(B-J)/2}P_{+1}(l+J;d)P_{-1}(l;d)P_0(B-2l-J;d)\frac{B!}{l!(l+J)!(B-2l-J)!} \\ &\sim \mathcal{N}(0,\sigma_J(d,B)).\end{aligned} \tag{23}$$

The last asymptotic holds for large B; the null mean value $\langle J\rangle_{d,B}=0$ is due to the symmetry characterizing $P(\xi_i^\mu)$ (see Eq. 9), while the standard deviation is $\sigma_J=\sqrt{\langle J^2\rangle_{d,B}}=\sqrt{B}(1-d)$.

The full solution of the previous equation reads as $P(J;d,B)=x^J\binom{B}{J}[d(2-d)]^B\,{}_2F_1[-(B-J)/2,-(B-J-1)/2,1+J,4x^2]$, where $x=(1-d)^2/[2d(2-d)]$. An explicit, exact expression for this probability can be written for a particular value of d, by exploiting Gauss's Hypergeometric Theorem [13], so that when $4x^2=1$, corresponding to $d=1-\sqrt{2}/2\approx 0.293$, we have

$$P(J;1-\sqrt{2}/2,B)=4^{-B}\binom{2B}{B+J}\sim\frac{e^{-J^2/B}}{\sqrt{\pi B}}. \tag{24}$$

In the last passage we used the Stirling approximation assuming $B \pm J$ large, namely that the distribution is peaked on non-extreme values of J.

It is worth underlining that $P(J; d, B)$ does not depend on the size H. Indeed, patterns are drawn independently and randomly so that the coupling J_{ij} may be regarded as the distance covered by a random walk of length B and endowed with a waiting probability $d(2-d)$. Hence, the end-to-end distance is distributed normally around zero and with variance (mean squared distance) which is given by the diffusion law, namely $\sim B$. The possibility of the walker to stop simply reduces the effective walk length to $[(1-d)(2-d)]B = (1-d)^2 B$ in agreement with results above.

3.3 Pattern dilution versus Topological dilution

Dilution on pattern entries does not necessarily yield to a topological dilution for the associative network, but, as we will see, can induce non-trivial cooperative effects. On the other hand, a topological dilution can be realized by directly cutting the edges on a standard Hopfield network. In this section we highlight the deep difference between these two kinds of dilution.

First, we recall that, according to a mean-field approach, the network is expected to display a giant component when the average link probability is larger than $1/H$. In the thermodynamic limit and assuming a large enough size B (stemming from either low, i.e. $B \sim \log H$, or high, i.e. $B \sim H$, storage regimes) to ensure the result in Eq. (23) to hold, for any finite value of d the emergent graph turns out to be always over-percolated. In fact, $P_{\text{link}}(d, B) = 1 - P(J = 0; d, B) \sim 1 - 1/\sqrt{2\pi\sigma_J^2}$, so that it suffices that $\sigma_J > H/[\sqrt{2\pi}(H-1)] \to 1/\sqrt{2\pi}$ and this leads to $d < 1 - (2\pi B)^{-1/2} \to 1$.

On the other hand, when B is finite we can check the possible disconnection of the network by studying $P(J = 0; d, B)$ from Eq. 20 and we get that $P_{\text{link}}(d, B) < 1/H$ for $d > 1 - 1/\sqrt{BH}$. Thus, in the thermodynamic limit, for any finite d, the graph is still overpercolated. Replacing $1/H$ with $(\log H)/H$, one also finds that the graph is even always connected.

Different scenarios may emerge if we take d properly approaching to 1 as H is increased [2].

Another kind of dilution can be realized by directly cutting edges in the resulting associative network, as for instance early investigated in the neural scenario by Sompolinsky on the Erdös-Renyi graph [48, 5] or more recently by Coolen and coworkers on small worlds and scale-free structures [52, 44].

Such different ways of performing dilution - either on links of the associative network (see [48, 5, 52, 44]) or on pattern entries (see Eq. 4) - yield deeply different thermodynamic behaviors. To see this, let us consider the field insisting on each spin, namely for the generic i^{th} spin $\varphi_i = \sum_{i \neq j=1}^{N} J_{ij}\sigma_j$, and analyze its distribution $P(\varphi|d)$ at zero noise level. When dilution is realized on links (d is the fraction of links cut), only an average fraction d of the H available spins participates to φ, in such a way that both the peak and the span of the distribution decrease with d (Fig. 3, left). Conversely, when dilution is realized on the underlying bi-layer (d is the fraction of null entries in a pattern), as $d > 0$, $P(\varphi|d)$ gets broader and peaked at smaller values of fields. The latter effect is due to the fact that couplings are, on average, of smaller magnitude. As for the former effect, we notice that, at β, H and B fixed, when dilution is introduced in bit-strings, couplings are made *uniformly* weaker (this effect is analogous to a rise in the fast noise) so that the distribution of spin configurations, and consequently also $P(\varphi|d)$, gets broader. At small values of dilution this effect dominates, while at larger values the overall reduction of coupling strengths prevails and fields get not only smaller but also more peaked (Fig. 3, right).

4 Parallel processing performances

4.1 Statistical mechanics of the low-storage case

As a minimal bibliography in the statistical mechanics approach, we report that a different study sharing some similarities with our work, investigates an associative network with pattern inhibition (due to chemical modulation) in neuroscience scenario and has been performed in [18][19], while a macroscopic behavior close to parallel processing were already reported in [20], where more than one magnetization were able to retain strictly positive values owing to strong pattern correlations (a completely different motivation).

Now, we solve the model in the regime $B \sim \log H$, such that the limit $\alpha = \lim_{H\to\infty} B/H = 0$. Like in the Amit-Gutfreund-Sompolinsky (AGS) neural network [5], the comprehension of the non-saturated case is the first fundamental step to face before moving to the saturated case. This can be accomplished in several ways: We use the approach performed in [17].

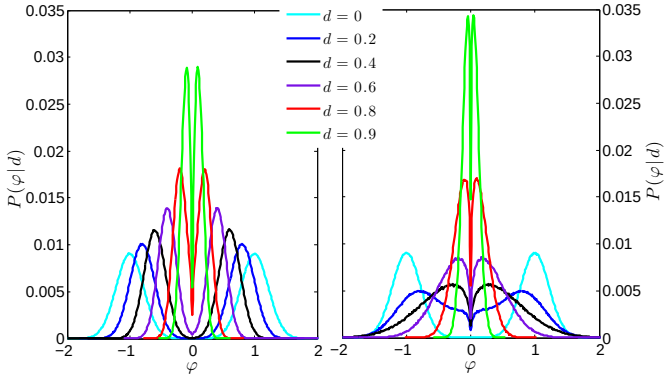

Figure 3: Left panel: Distribution of the field φ acting on the helpers with (Sompolinsky) dilution in the directed network [H-H]. Right panel: Distribution of the field φ acting on the helpers with (our) dilution in the bi-layered network [B-H].

Considering the pattern overlaps, also called generalized Mattis magnetization,

$$m_\mu = \frac{1}{H}\sum_i^H \xi_i^\mu h_i, \tag{25}$$

it is possible to rewrite the Hamiltonian (15) as

$$\tilde{\mathcal{H}}(h;\xi) = -\frac{H}{2}\sum_{\mu=1}^{B} m_\mu^2(h) + \frac{1}{2}B, \tag{26}$$

where we emphasized that the Mattis magnetizations are functions of the helpers.
These order parameters (properly averaged) are extremely useful to quantify the phases of the system as they are zero when the system displays no collective capabilities in orchestrating a response and differ from zero otherwise.
We introduce three types of average: the Boltzmann average $\omega(m_\mu) = \sum_h m_\mu \exp(-\beta\tilde{\mathcal{H}}(h;\xi))/Z_{H,B}(\beta,d)$, the average $\mathbb{E}$ performed over the quenched disordered couplings ξ and the global expectation $\mathbb{E}\omega(m_\mu)$ defined by the brackets $\langle m_\mu\rangle$.

The equilibrium equations for the order parameter can be obtained from the quenched free energy $\langle F(\beta,d)\rangle$

$$\langle F(\beta,d)\rangle = -\lim_{H\to\infty}\frac{1}{\beta}\mathbb{E}\log Z_{H,B}(\beta,d) = -\lim_{H\to\infty}\frac{1}{\beta}\mathbb{E}\log\sum_{\{h\}}^{2^H} e^{-\beta\tilde{\mathcal{H}}(h;\xi)}. \tag{27}$$

Introducing the notation $\mathbf{m} = (m_1,...,m_B)$ and $\xi_\mathbf{i} = (\xi_i^1,...,\xi_i^B)$ the above equation can be expressed in

terms of the density of state $\mathcal{D}(\mathbf{m})$

$$\mathcal{D}(\mathbf{m}) \equiv \sum_{\{h\}}^{2^H} \delta(\mathbf{m} - \mathbf{m}(h)), \tag{28}$$

as

$$Z_{H,B}(\beta, d) = \int d\mathbf{m} Z(\mathbf{m}), \quad Z(\mathbf{m}) = e^{H\beta \mathbf{m}^2/2} \mathcal{D}(\mathbf{m}).$$

Note further that the delta function here is a product of independent delta functions, once for each B-clone, namely:

$$\delta\left(\mathbf{m} - \mathbf{m}\left(h\right)\right) = \prod_{\mu=1}^{B} \delta\left(m_\mu - m_\mu\left(h\right)\right).$$

We need now to introduce B integration variables $\mathbf{x} = (x_1, ..., x_B)$ to switch the delta functions to their integral representation as

$$\mathcal{D}(\mathbf{m}) = \left(\frac{H}{2\pi}\right)^B \int d\mathbf{x} e^{iH\mathbf{x}\cdot\mathbf{m}} \sum_{\{h\}}^{2^H} e^{-i\sum_i^H \sum_\mu^B h_i \xi_i^\mu x_\mu} = \left(\frac{H}{2\pi}\right)^B \int d\mathbf{x} e^{H(i\mathbf{x}\cdot\mathbf{m} + \langle \ln 2\cos(\mathbf{x}\cdot\xi)\rangle_\xi)},$$

where we assumed the property $\lim_{H\to\infty} \sum_i^H f(\xi_\mathbf{i})/H = \langle f(\xi)\rangle_\xi$.
Physically speaking, the log-density of the states quantifies the constrained entropy $S(\mathbf{m})$ and can now be evaluated trough saddle point integration because of the factor H in the exponent of its integral representation above. Strictly speaking, we calculate only the leading term of the density of states, which however is the only retaining statistical meaning in the thermodynamic limit and is given by the maximum over $\mathbf{x}$ of $S(\mathbf{x}, \mathbf{m})$, the latter being

$$S(\mathbf{x}, \mathbf{m}) = i\mathbf{x}\cdot\mathbf{m} + \langle \ln 2\cos(\mathbf{x}\cdot\xi)\rangle_\xi.$$

It is then clear that the intensive quenched free energy can be rewritten as

$$\lim_{H\to\infty} \langle F(\beta, d)/H\rangle = -\frac{1}{\beta}\log 2 - \lim_{H\to\infty} \frac{1}{H\beta} \int d\mathbf{m} \mathcal{D}(\mathbf{m}) e^{\frac{1}{2}\beta H \mathbf{m}^2}. \tag{29}$$

The main contribution to free energy can be made explicit as a finite-dimensional integral; as outlined before for the constrained entropy, trough the extensively linearity property of thermodynamic observables, for large value of H the integral will be dominated by the saddle-point that maximizes the exponent as

$$\lim_{H\to\infty} \langle F(\beta, d)/H\rangle = -\lim_{H\to\infty} \frac{1}{H\beta} \int d\mathbf{m}\, d\mathbf{x} e^{-H\beta f(\mathbf{x},\mathbf{m})} = \mathrm{extr}[f(\mathbf{x}, \mathbf{m})], \tag{30}$$

$$f(\mathbf{x}, \mathbf{m}) = -\frac{1}{2}\mathbf{m}^2 - i\mathbf{x}\cdot\mathbf{m} - \frac{1}{\beta}\langle \log 2\cos[\beta\xi\cdot\mathbf{x}]\rangle_\xi. \tag{31}$$

To identify the various ergodic components (which are expected to be $B+1$, one being the paramagnetic) we find the stationary points of $f(\mathbf{m})$ trough the system $\partial_{m_\mu} f(\mathbf{m}) = 0$ for all $\mu \in (1, ..., B)$, which gives the vectorial self-consistence equations

$$\mathbf{x} = i\beta\mathbf{m}, \qquad i\mathbf{m} = \langle \xi \tan[\xi\cdot\mathbf{x}]\rangle_\xi. \tag{32}$$

Being the saddle point values of $\mathbf{x}$ purely imaginary, and using $\tanh(x) = -i\tan(ix)$ we get

$$\mathbf{m} = \langle \xi \tanh[\beta\xi\cdot\mathbf{m}]\rangle_\xi. \tag{33}$$

Then, the above equation has to be averaged over the pattern distribution $P(\xi_i^\mu)$ and finally solved numerically, as explained for the following few examples[8].

Before proceeding it is worth noticing that the Hamiltonian $\mathcal{H}(h;\xi)$ of Eq. (26) is quadratic in the Mattis magnetizations and the B stored patterns contain (on average) a fraction d of null entries. As a consequence, the pure state ansatz ($m_1 = 1, m_2 = ... = m_B = 0$) [5] can no longer work. In fact, now, the retrieval of a pattern (say ξ^1, the one coupled to m_1) does not employ all the available helpers (and coherently m_1 is strictly smaller than one for $d \neq 0$) and those corresponding to null entries can be used

[8]Despite the structure of the self-consistencies for general B retrieved patterns are extremely simple both conceptually and analytically, they become, already for $B > 3$, of prohibitive length and handleable only via calculators.

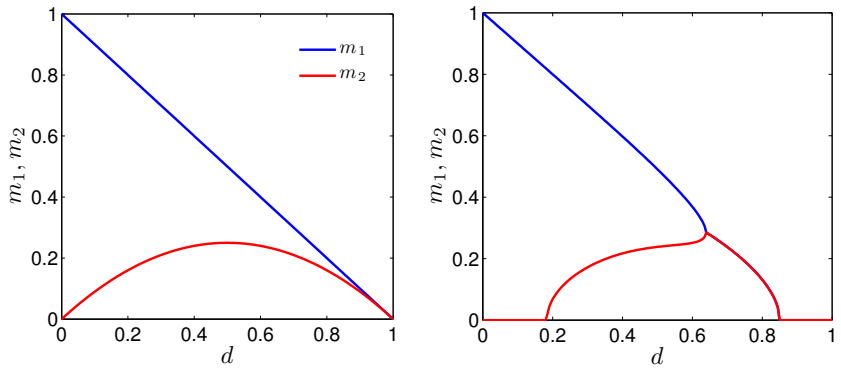

Figure 4: Behavior of the two Mattis magnetizations m_1 and m_2 versus d at two (small) noise levels, namely $\beta^{-1} = 10^{-4}$ (left panel) and $\beta^{-1} = 0.05$ (right panel).

to recall other patterns. As the energy is a quadratic form in the Mattis magnetizations, its minimization requires that further patterns (up to the exhaustion of all available helpers) are recalled in a hierarchical fashion. More precisely, the (thermodynamical and quenched) average of the Mattis magnetization of the k^{th} pattern retrieved scales as $d^k(1-d)$, that is the overlap with the free helpers still available is maximized. The overall number of retrieved patterns K therefore corresponds to $\sum_{k=0}^{K} d(1-d)^k = 1$, with the cut-off at finite H by $d(1-d)^K \geq H^{-1}$ due to discreteness. For any fixed and finite d, this implies $K \lesssim \log H$, which can be thought of as a "parallel low-storage" regime. In other words, once m_1 has been retrieved, it is energetically convenient for the system to coordinate its free helpers to align with another pattern (the one denoted by ξ^2) instead of letting them align randomly.

4.2 The case $B = 2$

The self-consistencies encoded into Eq. (33) for the simplest case $B = 2$ are

$$m_1(\beta, d) = d(1-d)\tanh(\beta m_1) + \frac{(1-d)^2}{2}\big[\tanh[\beta(m_1+m_2)] + \tanh[\beta(m_1-m_2)]\big], \tag{34}$$

$$m_2(\beta, d) = d(1-d)\tanh(\beta m_2) + \frac{(1-d)^2}{2}\big[\tanh[\beta(m_1+m_2)] - \tanh[\beta(m_1-m_2)]\big]. \tag{35}$$

The solution of these equations for different values of β is reported in Fig. (4). In the low (fast) noise limit ($\beta \to \infty$), when no dilution is present ($d = 0$) the second magnetization m_2 disappears and the first magnetization m_1 approaches the value 1 as expected because the Hopfield model is recovered. As dilution is increased, m_1 decreases linearly, while m_2 displays a parabolic profile with peak at $d = 0.5$. In the presence of (fast) noise, m_2 starts growing for higher values of dilution because (as will be cleared by the signal-to-noise analysis of the next section) the signal[9] insisting on the latter, which is proportional to $d(1-d)$, must be higher than the noise level in order to be effective. Also notice that, from intermediate dilution onwards, m_1 and m_2 collapse and the related curves converge at a "bifurcation" point.
Let us now deepen these results, first from a more intuitive point of view, and later from a more rigorous one.

In the zero (fast) noise limit, let us fix ξ^1 as the pattern corresponding to the maximum overlap with the magnetic configuration, so that the expected Mattis magnetization is $\langle m_1 \rangle = (1-d)$. The remaining $H\,d$ "free" spins will seek for patterns to align with, namely displaying non-null entries in correspondence with the null entries of ξ^1. Actually, due to dilution, one expects that the second best-matching pattern only engages $H\,d(1-d)$ spins, while the remaining $H\,d^2$ will match other patterns; in general, the k-th best-matching pattern is expected to engage $H\,d^{k-1}(1-d)$.

Such a hierarchical fashion for alignment is more optimal than a uniform alignment of spins amongst the available patterns which would yield $m_k = d/B$ for any k and an overall energy $-H/2\sum_k (d/B)^2 = -(d^2 H)/(2B)$. Indeed, the hierarchical solution is the one that minimizes the energy (recall that the magnetization are summed quadratically) as well as the most likely from a combinatorics point of view, providing an overall energy $-H/2\sum_k [(1-d)d^k]^2 = -H(1-d^{2+2B})(1-d)/[2(1+d)]$.

Therefore, the system is able to perform the "parallel retrieval" of K patterns, whose magnetizations are $m_\mu = (1/H)\sum_i \xi_i^\mu h_i$, that is $\langle m_1 \rangle = (1-d)$, $\langle m_2 \rangle = d(1-d)$, ..., $\langle m_K \rangle = d^K(1-d)$. It is easy

[9] We use the term "fields" for the forces acting on h_i and "channels" for those on m_μ.

to see that it must be $d^{K+1} = 0$. Hence, for any finite value of d, an infinite number of patterns can in principle be retrieved, i.e. $d^K \to 0$, for $K \to \infty$. More accurately, taking into account the discreteness of the system, we have that the last pattern to be retrieved will match only one helper, which yields $H\, d^K(1-d) = 1$, from which $K = [\log H + \log(1-d)]/\log(1/d) \sim \log H$. In the low storage regime, with B finite or scaling logarithmically with H, the retrieval of all patterns can, in principle, always be accomplished.
When noise is also introduced, we have that for the i-th pattern to be retrieved the field felt by helpers has to be larger than the noise level, that is $[d(1-d)^i] > \beta^{-1}$, if this condition is not fulfilled the field is confused with the noise and the pattern can not be retrieved.

In the case of large degree of dilution, i.e. d close to 1, patterns are so sparse that not all the H helpers can be matched; assuming that patterns get orthogonal, only a fraction $B(1-d)/H$ ($= \alpha(1-d)$ or $= \alpha \log H(1-d)/H$ in low and high storage regime, respectively) of helpers is aligned with a given pattern, the remaining are free and their mean value is zero. In this condition the emergent graph is also disconnected.

Beyond constraints on d, probably the most striking feature displayed by m_1, m_2 is the bifurcation occurring at intermediate values of dilution (see Fig.4). In order to understand this phenomenon we can divide spins into four sets: $\mathcal{S}_1$, which contains spins i corresponding to zero entries in both patterns ($\xi_i^1 = \xi_i^2 = 0$), therefore behaving paramagnetically; $\mathcal{S}_2$, which includes spins seeing only one pattern ($|\xi_i^1| \neq |\xi_i^2|$); $\mathcal{S}_3$, which contains spins corresponding to two parallel, non-null entries ($\xi_i^1 = \xi_i^2 \neq 0$), thus being the most stable; $\mathcal{S}_4$, which includes spins i corresponding to two parallel, non-null entries ($\xi_i^1 = -\xi_i^2 \neq 0$), hence intrinsically frustrated.
The cardinality of these sets are: $|\mathcal{S}_1| = d^2$, $|\mathcal{S}_2| = 2d(1-d)$, $|\mathcal{S}_3| = (1-d)^2/2$, and $|\mathcal{S}_4| = (1-d)^2/2$. Now, the most prone spin to align with the related patterns are those in $\mathcal{S}_3$ and in $\mathcal{S}_2$, and this requires $(1-d) < \beta^{-1}$ for the field to get effective. As d is further reduced, m_1 and m_2 grow paired, due to the symmetry of the sets $\mathcal{S}_2$ and $\mathcal{S}_3$. The growth proceeds paired until the magnetizations get the value $m_1 = m_2 = (1-d)^2/2 + d(1-d)$, where the two contributes come from spins aligned with both patterns and with the unique pattern they see, respectively. From this dilution onwards frustrated spins also start to align so that one magnetization necessarily prevails over the other. This explanation can be extended to any finite B and, in general, the number of sets turns out to be $P + 1 + \sum_{k=0}^{B} \lfloor \frac{P-k}{2} \rfloor$.

Now we want to quantify these bifurcation points, and to this task let us call

$$x = \langle m_1 \rangle - \langle m_2 \rangle. \tag{36}$$

We use Eqs. (34) and (35) and expand for small values of x

$$\langle m_1 \rangle - \langle m_2 \rangle = x = d(1-d)[\tanh(\beta\langle m_1 \rangle) - \tanh(\beta\langle m_2 \rangle)] + (1-d)^2 \tanh\left(\beta\langle m_1 \rangle - \langle m_2 \rangle\right), \tag{37}$$

where

$$d(1-d)\left[\tanh\left(\beta\langle m_1 \rangle\right) - \tanh\left(\beta\langle m_2 \rangle\right)\right] \sim d(1-d)\left[\tanh(\beta\langle m_1 \rangle) - \tanh(\beta\langle m_2 \rangle) + \frac{\beta x}{\cosh^2(\beta\langle m_1 \rangle)}\right], \tag{38}$$

and

$$(1-d)^2 \tanh(\beta\langle m_1 \rangle - \langle m_2 \rangle) \sim (1-d)^2 \beta x + O(x^3). \tag{39}$$

Thus, the leading term is

$$x \sim \left[\frac{d(1-d)\beta}{\cosh^2(\beta\langle m_1 \rangle)} + \beta(1-d)^2\right] x. \tag{40}$$

The critical value of β corresponding to the bifurcation point is defined as

$$\beta_c^{bif} = \frac{1}{(1-d)^2\left[1 + \frac{(1-d)}{d}\frac{1}{\cosh^2(\beta_c^{bif} m_1)}\right]}. \tag{41}$$

This mechanism can be easily generalized to the case of multiple patterns.

We move now to analyze the critical noise level at which the magnetizations disappear and the network dynamics becomes ergodic, still in this test-case of two patterns: Expanding expressions (35) we find

$$\begin{aligned}\langle m_2 \rangle \;&\sim\; d(1-d)[\beta\langle m_2 \rangle] + \frac{(1-d)^2}{2}[\beta\langle m_1 \rangle + \beta\langle m_2 \rangle + \frac{\beta^3}{3}(\langle m_1 \rangle^3 + \langle m_2 \rangle^3 + 3\langle m_1 \rangle^2\langle m_2 \rangle + 3\langle m_1 \rangle\langle m_2 \rangle^2)] + \\ &+\; d(1-d)\frac{\beta^3}{3}\langle m_2 \rangle^3 - \frac{(1-d)^2}{2}[\beta\langle m_1 \rangle - \beta\langle m_2 \rangle + \frac{\beta^3}{3}(\langle m_1 \rangle^3 - \langle m_2 \rangle^3 - 3\langle m_1 \rangle^2\langle m_2 \rangle + 3\langle m_1 \rangle\langle m_2 \rangle^2)],\end{aligned}$$

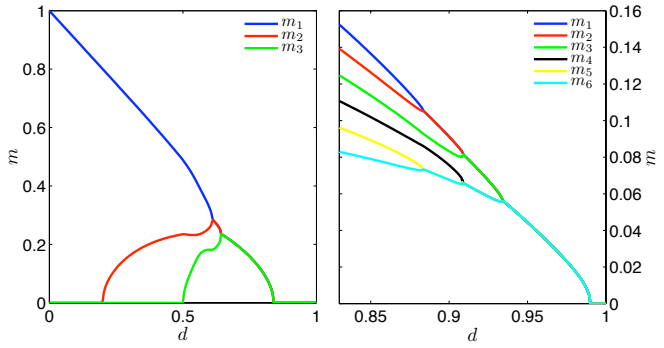

Figure 5: Parallel retrieval of three (left panel) and of six (right panel) patterns. Behavior of the two Mattis magnetization versus d at noise level $\beta^{-1} = 0.05$.

such that we can write

$$\langle m_2 \rangle \sim (1-d)\beta\langle m_2 \rangle + \mathcal{O}(\langle m_2 \rangle^3). \tag{42}$$

Therefore the critical noise level turns out to be

$$\beta_c = \frac{1}{1-d}. \tag{43}$$

This calculation can easily be generalized to several patterns, too.

4.3 The case $B = 3$

When three patterns are considered, the related self-consistent equations that constraint the system to parallel processing are the following (we skip the brackets $\langle . \rangle$ for the sake of clearness):

$$\begin{aligned} m1 &= d^2(1-d)\tanh[\beta m1] - (1/4)d(1-d)^2\tanh[\beta(-m1-m2)] + \\ &+ (1/4)d(1-d)^2\tanh[\beta(m1-m2)] - (1/4)d(1-d)^2\tanh[(-m1+m2)] + \\ &+ (1/4)d(1-d)^2\tanh[\beta(m1+m2)] - (1/4)d(1-d)^2\tanh[\beta(-m1-m3)] + \\ &- (1/4)d(1-d)^2\tanh[\beta(m1-m3)] - (1/8)(1-d)^3\tanh[\beta(-m1-m2-m3)] + \\ &+ (1/8)(1-d)^3\tanh[\beta(m1-m2-m3)] - (1/8)(1-d)^3\tanh[\beta(-m1+m2-m3)] + \\ &+ (1/8)(1-d)^3\tanh[\beta(m1+m2-m3)] - (1/4)d(1-d)^2\tanh[\beta(-m1+m3)] + \\ &+ (1/4)d(1-d)^2\tanh[\beta(m1+m3)] - (1/8)(1-d)^3\tanh[\beta(-m1-m2+m3)] + \\ &+ (1/8)(1-d)^3\tanh[\beta(m1-m2+m3)] - (1/8)(1-d)^3\tanh[\beta(-m1+m2+m3)] + \\ &+ (1/8)(1-d)^3\tanh[\beta(m1+m2+m3)]] \end{aligned} \tag{44}$$

$$\begin{aligned} m2 &= -(1/4)d(1-d)^2\tanh[\beta(-m1-m2)] - (1/4)d(1-d)^2\tanh[\beta(m1-m2)] + \\ &+ d^2(1-d)\tanh[\beta m2] + (1/4)d(1-d)^2\tanh[\beta(-m1+m2)] + \\ &+ (1/4)d(1-d)^2\tanh[\beta(m1+m2)] - (1/4)d(1-d)^2\tanh[\beta(-m2-m3)] - \\ &- (1/8)(1-d)^3\tanh[\beta(-m1-m2-m3)] - (1/8)(1-d)^3\tanh[\beta(m1-m2-m3)] + \\ &+ (1/4)d(1-d)^2\tanh[\beta(m2-m3)] + (1/8)(1-d)^3\tanh[\beta(-m1+m2-m3)] + \\ &+ (1/8)(1-d)^3\tanh[\beta(m1+m2-m3)] - (1/4)d(1-d)^2\tanh[\beta(-m2+m3)] - \\ &- (1/8)(1-d)^3\tanh[\beta(-m1-m2+m3)] - (1/8)(1-d)^3\tanh[\beta(m1-m2+m3)] + \\ &+ (1/4)d(1-d)^2\tanh[\beta(m2+m3)] + (1/8)(1-d)^3\tanh[\beta(-m1+m2+m3)] + \\ &+ (1/8)(1-d)^3\tanh[\beta(m1+m2+m3)]] \end{aligned} \tag{45}$$

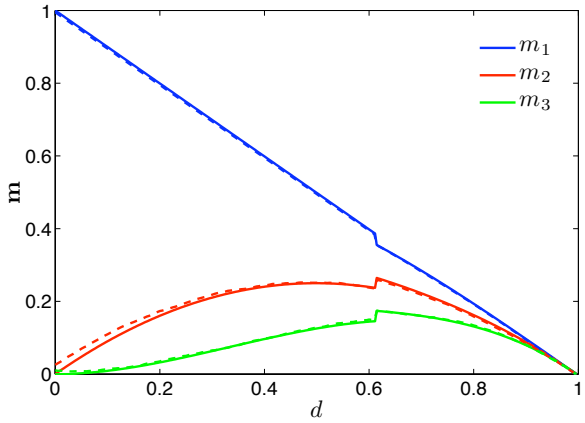

Figure 6: Parallel retrieval of three strategies. Behavior of three Mattis magnetization versus d in the slow (fast) noise limit (i.e. $\beta^{-1} = 10^{-4}$). Continuous lines correspond to numerical solution of Eqs. (44)-(46), while dashed lines correspond to Monte Carlo simulations.

$$\begin{aligned} m3 &= -(1/4)d(1-d)^2\tanh[\beta(-m1-m3)] - (1/4)d(1-d)^2\tanh[\beta(m1-m3)] - \\ &- (1/4)d(1-d)^2\tanh[\beta(-m2-m3)] - (1/8)(1-d)^3\tanh[\beta(-m1-m2-m3)] - \\ &- (1/8)(1-d)^3\tanh[\beta(m1-m2-m3)] - (1/4)d(1-d)^2\tanh[\beta(m2-m3)] - \\ &- (1/8)(1-d)^3\tanh[\beta(-m1+m2-m3)] - (1/8)(1-d)^3\tanh[\beta(m1+m2-m3)] + \\ &+ d^2(1-d)\tanh[\beta m3] + (1/4)d(1-d)^2\tanh[\beta(-m1+m3)] + \\ &+ (1/4)d(1-d)^2\tanh[\beta(m1+m3)] + (1/4)d(1-d)^2\tanh[\beta(-m2+m3)] + \\ &+ (1/8)(1-d)^3\tanh[\beta(-m1-m2+m3)] + (1/8)(1-d)^3\tanh[\beta(m1-m2+m3)] + \\ &+ (1/4)d(1-d)^2\tanh[\beta(m2+m3)] + (1/8)(1-d)^3\tanh[\beta(-m1+m2+m3)] + \\ &+ (1/8)(1-d)^3\tanh[\beta(m1+m2+m3)]]. \end{aligned} \tag{46}$$

Recalling the picture explained in the previous subsection, the magnetizations m_1, m_2 and m_3 again grow together until all helpers corresponding to equal non-null entries and to single non-null entries are aligned. Then helpers which are aligned only with two patterns out of three start to feel the field and get aligned hence breaking the symmetry. At this point, say m_1 and m_2, still grow while m_3 decreases. The next symmetry-breaking occurs when all helpers corresponding to equal non-null entries $\xi^1 = \xi^2$ get aligned. From this point onward one magnetization prevails against the other. The same process applies, mutatis mutandis, for larger number of patterns (see Fig.5).

The last subtlety to be investigated is given by the small discontinuities in the behavior of the magnetizations (see for instance Fig.6). To explain this feature, let us consider the set of patterns $\xi_1, \xi_2, ..., \xi_B$ and assume the zero fast noise limit ($\beta \to \infty$) for the sake of simplicity, so that we can take $|m^k| = (1-d)d^{k-1}$, for $k = 1, ..., B$ as (absolute) Mattis magnetizations. The field insisting on the arbitrary helper h_i can be written as

$$\varphi_i = \frac{1}{H}\sum_{j\neq i}^{H} J_{ij}h_j = \sum_{\mu=1}^{B}\xi_i^\mu m^\mu - \frac{1}{H}\sum_{\mu=1}^{B}\xi_i^\mu\xi_j^\mu h_i \approx \sum_{\mu=1}^{B}\xi_i^\mu m^\mu, \tag{47}$$

where in the last passage we dropped the second sum as it is vanishing in the thermodynamic limit. Now, let us consider the spin h_1, which, again without loss of generality can be thought of as aligned with the first pattern and equal to $+1$. The field insisting on this lymphocyte is $\varphi_1 = (1-d)[1+\sum_{\mu=2}^{B}\epsilon(1,\mu)d^{\mu-1}]$, where $\epsilon(1,\mu) = \mathrm{sgn}(\xi_1^\mu, m^\mu)$. We notice that, in general, φ_1 is not positive definite so that the occurrence of the condition $\varphi_1 < 0$ would lead to the spin flip $h_1 = 1 \to h_1 = -1$ and, consequently, to $m_1 < (1-d)$. In order to understand this effect we focus on $\epsilon(1,\mu)$. By assumption, $m_1 = (1-d)$ and $h_1 = \xi_1^1$, so that the first entry of pattern $\mu = 1$ effectively contributes to the related magnetization m_1. As for the following magnetizations $m_{\mu>2}$, effective contributes can arise only from entries $\xi_j^{\mu>2}$ corresponding to null entries in ξ_j^1. Otherwise stated, there is no correlation between ξ_1^μ and m^μ for $\mu > 1$ (in fact, $\epsilon(1,\mu)$ is zero on average), and one can count the pattern configurations leading to $\varphi_1 < 0$ applying combinatorics.

Seeking for clarity, we consider the following explicit cases:

- The probability that the first entries of all patterns $\mu > 1$ are misaligned with respect to the related magnetizations is $[(1-d)/2]^{B-1}$, hence giving a field $\varphi_1 = (1-d)[1-\sum_{\mu>2}d^{\mu-1}] = 1-2d+d^{B+1}$. Such

a field turns out to be negative in the interval $a_1 < d < 1$, where $a_1 \to 1/2$ for $B \to \infty$.
- The probability that the first entries of all patterns $\mu > 1$ but one, say ξ^l, are misaligned and that $\xi^l_1 = 0$ is $d[(1-d)/2]^{B-2}$, and this would lead to $\varphi_1(l) = (1-d) - d(1-d^B) + (1-d)d^{l-1}$, which is negative for $a_2 < d < 1$, where $a_2 \to 1/2$ for $B \to \infty$; of course $\varphi_1(l)$ is growing with l.
- The probability that the first entries of all patterns $\mu > 1$ but one, say ξ^l, are misaligned and that $\xi^l_1 = 1$, is $d[(1-d)/2]^{B-1}$ and this configuration yields $\varphi_1(l) = (1-d) - d(1-d^B) + 2(1-d)d^{l-1}$. For instance, when $l = 2$ and $B \gg 1$, the field is negative for $d > 1/\sqrt{2}$; when $l = 3$ the field is negative for $d > a_3$, where $a_3 \approx 0.648$.
Summarizing, in the zero noise limit $\beta \to \infty$ for any given dilution d, the probability that $m_1 < (1-d)$ can be written as a sum over pattern configurations leading to $\varphi_1 < 0$. For instance, for $B = 3$, only one out of the 3^{B-1} possible configurations, i.e. $\mathrm{sgn}(\xi^\mu_2, m^\mu) = \mathrm{sgn}(\xi^\mu_3, m^\mu) = -1$, can yield a spin-flip: the corresponding field is $\varphi_1 = (1-d)(1-d-d^2)$, which is negative for $d > (\sqrt{5}-1)/2 \approx 0.62$ (see Fig. 6). Therefore, for that value of dilution onwards, m_1 is reduced with respect to the optimal value $(1-d)$. The extent of the loss is a fraction $1/9$ of the total, namely ≈ 0.34 (see Fig. 6).

Notice that while the change reduces m_1, other magnetizations are favored by the spin-flip and undergo a proportional increment. Also, the occurrence of a magnetization reduction with respect to the optimal value is more likely for the highest magnetization m_1, because fields insisting on spins contributing to m_1 are the most complex, being the sum of $B-1$ terms. The same discussion can be applied in turns to m_2: now the number of terms which sum up to give the field insisting on the $(1-d)d$ spins which contribute effectively to m_2 is $B-2$, so that there are far less configurations able to yield a negative field. Consequently, a loss in m_2 is less likely. Therefore, as long as the number of patterns allows readjustments in the value of magnetizations with respect to those expected, the arbitrary m_k may display complex corrections (possibly occurring at slightly different values of d) due to the combination of several simple corrections, each corresponding to the readjustment affecting the previous magnetizations $m_{\mu<k}$ (see Fig. 6).

4.4 Signal to noise ratio in the zero fast noise limit

As usually done in the neural network context [5], we couple the statistical mechanics inspection to signal-to-noise analysis. Aim of this procedure is trying to confirm the "parallel ansatz" we implicitly made by studying the stability of the basins of attractions (whose fixed points are the learned strategies) created in the hierarchical fashion we prescribed. We recall that the model we are investigating describes a low storage of information in the associative network so that no slow noise is induced by the underlying spin glass, i.e. $\alpha = 0$. Nonetheless, we study the signal to noise ratio in the zero fast noise limit ($\beta \to \infty$) as a problem formulated in general terms of α, d; then, we take the limit $\alpha \to 0$ to get estimate about the stability of the basins of attractions (where the presence of fast noise can possibly produce fluctuations).

Without loss of generality, we assume that the network is retrieving the first pattern. This means that spins are aligned with the non-null entries in the first bit-string ξ^1, while the remaining spins explore the other patterns. Thus, for the generic spin h_i we can write

$$h_i = \xi^1_i + \sum_{\nu=2}^{B} \xi^\nu_i \prod_{\mu=1}^{\nu-1} \delta(\xi^\mu_i). \tag{48}$$

Accordingly, the local field acting on the i^{th} lymphocyte can be written as

$$\varphi_i = \frac{1}{H} \sum_{j \neq i}^{H} \sum_{\mu}^{B} \xi^\mu_i \xi^\mu_j [\xi^1_j + \sum_{\nu=2}^{B} \xi^\nu_j \prod_{\mu=1}^{\nu-1} \delta(\xi^\mu_j)]. \tag{49}$$

- In the reference case $B = 1$, like for the pure states of the Hopfield network, we set

$$h_i = \xi^1_i + \delta(\xi^1_i) k_i, \tag{50}$$

  where k_i is a random variable uniformly distributed on the values ± 1 added to ensure that there are no nulls entries in the state of the network. Hence we find

$$\langle \varphi_i h_i \rangle_\xi = \langle signal + noise \rangle_\xi = \langle signal \rangle_\xi \tag{51}$$

  being $\langle noises \rangle_\xi = 0$, and so for large H we have

$$\langle signal \rangle_\xi = \frac{H-1}{H}(1-d) = (1-d), \tag{52}$$

while

$$\langle (noises)^2 \rangle_\xi = \frac{B-1}{H}(1-d)^2 = \alpha(1-d)^2. \tag{53}$$

- In the test case of two patterns retrieved, $B = 2$, we set:

$$h_i = \xi_i^1 + \delta(\xi_i^1)[\xi_i^2 + \delta(\xi_i^2)k_i]. \tag{54}$$

Now, we need to distinguish between the various possible configurations:

– $\forall i$ such that $\xi_i^1 \neq 0, \xi_i^2 = 0$ and so that $h_i = \xi_i^1 \neq 0$ for large value of H

$$\langle signal \rangle_\xi = (1-d), \quad \langle noises \rangle_\xi = 0, \tag{55}$$

$$\langle (noises)^2 \rangle_\xi = \frac{(H-1)(B-2)}{H^2}(1-d)^2 = \alpha(1-d)^2. \tag{56}$$

– $\forall i$ such that $\xi_i^1 \neq 0, \xi_i^2 \neq 0$ and so that $h_i = \xi_i^1 \neq 0$
if $\xi_i^1 = \xi_i^2$

$$\langle signal \rangle_\xi = 2(1-d) - (1-d)^2, \quad \langle noises \rangle_\xi = 0, \tag{57}$$

if $\xi_i^1 = -\xi_i^2$

$$\langle signal \rangle_\xi = (1-d)^2, \quad \langle noises \rangle_\xi = 0. \tag{58}$$

and in both cases

$$\langle (noises)^2 \rangle_\xi = \frac{(H-1)(B-1)}{H^2}(1-d)^3 + \frac{(H-1)(B-2)}{H^2}d(1-d)^2 = \alpha(1-d)^2.$$

– $\forall i$ such that $\xi_i^1 = 0, \xi_i^2 \neq 0$ and so that $h_i = \xi_i^2 \neq 0$

$$\langle signal \rangle_\xi = d(d-1), \quad \langle noises \rangle_\xi = 0, \tag{59}$$

$$\langle (noises)^2 \rangle_\xi = \frac{(H-1)(B-1)}{H^2}(1-d)^3 + \frac{(H-1)(B-2)}{H^2}(1-d)^2 d = \alpha(1-d)^2. \tag{60}$$

Therefore, in the regime of low storage of strategies we are exploring ($\alpha = 0$), the retrieval is stable, states are well defined and the amplitude of the signal on the first channel is order $(1-d)$ while on the second is of order $d(1-d)$, in perfect agreement with both the statistical mechanics analysis and Monte Carlo simulations.

Once proved that these parallel states exist, it would be interesting trying to understand deeper their structure in the configurational space. To this task let us fix a pattern ξ_i^1, with $i = 1, ..., H$, and a dilution d, in such a way that $H\,d$ of ξ^1 entries are expected to be null and the remaining $H(1-d)$ are expected to be half equal to $+1$ and half equal to -1. The number of helper configurations displaying maximum overlap with ξ^1 corresponds to the degeneracy induced by null entries, namely 2^{Hd}; all these configurations lay in an energy minimum because their Mattis magnetization is maximum (actually the same holds for the symmetrical configurations due to the gauge symmetry of the model).

Let us now generalize this discussion by introducing the number of configurations $n(m,d)$ whose overlap with the given pattern displays m misalignments in such a way that $n(m,d)$ is given not only by the degeneracy induced by null entries, but also by the degeneracy induced by the choice of m entries out of $H(1-d)$ which have to be mismatched. It is easy to see that $n(m,d) = 2^{Hd}\binom{H(1-d)}{m}$. Interestingly, for such configurations the signal felt by a spin i can be written as $\varphi_i = \xi_i^1[H((1-d)) - 2m]$ and the effect of the correction due to the m misalignments might be vanishing in the presence of a sufficiently large level of noise, so that the system is not restricted to the 2^{Hd} configurations corresponding to the minimum energy, but it can also explore all the configurations $n(m,d)$.

Therefore, we can count the number of configurations $\tilde{n}(x,d)$ exhibiting a number of misalignments, with respect to ξ^1, up to a given threshold x; in the presence of noise such configurations are all accessible, namely they all lay in the same "deep" minimum. Indeed, we can write $\tilde{n}(x,d) = \sum_{m=0}^{x} n(m,d)$; of course, for $x = H(1-d)$ we recover $\tilde{n}(x,d) = 2^H$. Moreover, when $x = H(1-d)/2$, we can exploit the identity $\sum_{k=0}^{i}\binom{2i}{k} = 1/2[4^i + \binom{2i}{i}]$ [24], and assuming without loss of generality $H(1-d)$ to be even we get

$$\tilde{n}(H(1-d)/2,d) = \sum_{m=0}^{x} n(m,d) = \frac{2^{Hd}}{2}\left[2^{H(1-d)} + \binom{H(1-d)}{H(1-d)/2}\right] \approx \frac{2^H}{2}\left[1 + \sqrt{\frac{2}{\pi H(1-d)}}\right], \tag{61}$$

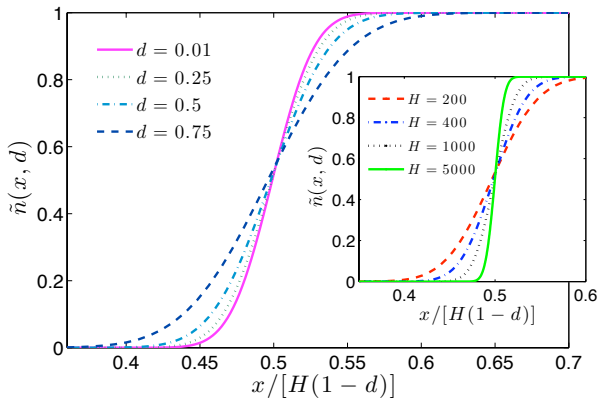

Figure 7: (Color on line) Normalized number of accessible configurations $\tilde{n}(x,d)$ as a function of x and d for a system made up of $H =$ lymphocytes. The critical line $x_c = (1-d)$, corresponds to the emergence of a giant component.

where in the last passage we used the Stirling approximation given that $H((1-d)) \gg 1$. Then, we have $\tilde{n}(H(1-d)/2, d) \gtrsim 1/2$, and similar calculations can be drawn for smaller thresholds, e.g., $\tilde{n}(H(1-d)/2 - 1, d) \lesssim 1/2$.

As shown in Fig. 7, once d is fixed, when x is small only a microscopic fraction $\tilde{n}(x,d)/2^H$ of configuration is accessible (in the thermodynamic limit this fraction is vanishing), while by increasing the tolerance x, more and more configuration get accessible and correspondently their fraction gets macroscopic. From a different perspective, each configuration can be looked at as a node of a graph and those accessible are connected together. The link probability is then related to x and when x is large enough a "giant component" made up of all accessible configurations emerges. This is a percolation process in the space of configurations. Indeed, similarly to what happens in canonical percolation processes, the curves representing the giant component relevant to different sizes H intersect at around $1/2$, which distinguishes the percolation threshold x_c. According to Eq. 61 we can write $x_c \approx H(1-d)/2$.

Interestingly, when a giant component emerges retrieval is no longer meaningful because the system may retrieve essentially anything and this corresponds to the critical line (in the d, β plane) where all the magnetization simultaneously disappear.

5 Numerics

In this Section we discuss details on Monte Carlo simulations.
All the simulations have been performed on a system Ubuntu Linux with Intel Core I7, 3.2Ghz, 12 CPU, Nvidia-Fermi technology, 12 Gb RAM and OpenMP libraries. The simulations were carried out sequentially according to the following algorithm:

1. Building and storaging of the coupling matrix.

   First, we generate B patterns according to the distribution ($d = 0$):

   $$P(\xi_i^\mu) = \frac{1}{2}\delta_{(\xi_i^\mu - 1)} + \frac{1}{2}\delta_{(\xi_i^\mu + 1)}, \tag{62}$$

   then, we build a char-matrix $J_{ij} = \sum_\mu \xi_i^\mu \xi_j^\mu$ with entries ranging $\in [0, 2B+1]$ and acting as key pointing to another hash-matrix $\tilde{J}_{ij}$ where the $H(H-1)/2$ real numbers accounting for the Hebb interactions (see eq. (16)) are stored. If the amount of patterns do not exceed $B = 256$, i.e. one byte, it is then possible to account for 10^5 helpers with no need of swapping on hard disk (which would sensibly affect the performance of the simulation). This condition is fulfilled for the low storage regime we are interested in.

2. Initialize the network status.

   We checked the two standard approaches: The first is to initialize the network in a (assumed) fixed point of the dynamics, namely

   $$h_i = \xi_i^1 \quad \forall i \in [1, ..., H] \tag{63}$$

and check its evolution: This gives important information on the structure of the basins of attraction of the minima as we vary the dilution (see Point 5).

The second approach is to initialize the network randomly: We set $h_i = 1$ with probability 0.5 and $h_i = -1$ otherwise. This is a standard procedure to follow the relaxation to a fixed point with no initial assumption and gives important information on the structure of the basins of attraction of the minima at fixed dilution.

3. Evolution dynamics

   The activity of helpers evolves according to a standard (random and sequential) Glauber dynamics for Ising-like systems [5]: At each time interval, the state of a lymphocyte is updated according to its input signals, where the probability of the unit's activity is equal to a rectified value of the input (logit transfer function), i.e.

$$Pr(h_i(t) = \pm 1) = \frac{1}{1 + \exp[\mp 2\beta \sum_j J_{ij} h_j].} \tag{64}$$

   The field-updating process is managed by a linked list whose parsing is parallelized through OpenMP.

4. Convergence of the simulation.

   Due to the peculiar structure of the fields induced by pattern dilution (see Fig. 3, right panel), the field insisting on a given helper may be zero and the related spin would flip indefinitely. To avoid this pathological situation we skip the updating of these "paramagnetic" lymphocytes and focus on the remaining ones: In the zero noise limit convergence is almost immediate, such that when the whole ensemble of helpers remains unchanged for the whole N-length of the update cycle, dynamics is stopped and the resulting B Mattis magnetizations are printed on a file.

   Relaxation at non-zero noise is checked through the linked list (see next step): The pointer of each helper that is aligned with its own field is stored, the ones of helpers with no net fields are removed from the linked list, while all the other helpers mismatched to their own fields, are added into the linked list.

5. Increase of B pattern dilution.

   There can be two deeply different ways of increasing dilution. The former is a Bernoullian approach and essentially if one starts from a dilution $d = 0.45$ toward a dilution $d = 0.5$ essentially may forget the starting information and generate a random pattern with on average one half of zero entries; the latter is a Markovian dilution by which one needs to start from the previous coupling matrix (and patterns) diluted at $d = 0.45$ and increases dilution on that structure.
   Dilution is tuned at steps of 0.01, ranging from $d = 0$ to $d = 1$.
   We take as the state of the network the last equilibrium state, then go to point (3).

Trough Markovian dilution, we can follow the evolution, varying d, of the pure Hopfield attractors[10]. Examples of results obtained via numerical simulations can be seen in Fig. 6 and are in general in perfect agreement with theory.

6 Summary and outlooks

In this paper we continued our modeling of immune networks through statistical mechanics. In particular, we recently proposed a model for the adaptive immune response by which helpers and B-cells interact via cytokines and are described as a fully-connected bipartite spin glass. We also showed that the model is equivalent to an attractor associative network where helpers are able to arrange B-cells and orchestrate responses; we underline that this first network was able to elaborate only one strategy at a time, namely, helpers managed only one clonal lineage of B-cells before turning to another one.

Here we introduce dilution in the bipartite spin-glass such that only a fraction of the whole B-repertoire interacts with a given helper lineage, which is a much more biological description and we obtain remarkable emergent behavior. At first, we have shown that diluting the bipartite B-H spin-glass is very different from diluting directly the resulting H-H associative network. In particular, while in the latter the peak of the distribution of the fields insisting on the dynamical variables is a monotone decreasing function

[10] Trough this dynamics, the bifurcation tree on dilution is obtained: Note the similarity among the self-consistence equations (see e.g. Eq.s (36, 37)) and the logistic map.

as dilution is increased, the former -our dilution- shows a minimum (as a function of noise level) and a high non trivial behavior. This hides in fact a new important property of these networks: They develop, as an emerging feature, the ability of retrieval of multiple strategies together; namely helpers are able to orchestrate and coordinate the responses of several B-clones at the same time.
Remarkably, each time the network of helpers retrieves patterns/strategies for (the correct) B-cell expansions, the corresponding Mattis magnetization is maximized (e.g. each helper belonging to the retrieval has the same sign of the cytochine linking it to the B-clone). This means that the field that insists on the B-clone, which on average (when no retrieval exists) is zero, becomes $\sim (1-d) > 0$ such that each retrieval in the helper network generates a "magnetic field" on the B-clone (in the B-H network) and consequenly the latter is forced to expand.
Another interesting remark is that the strength of the field increases as dilution is decreased: This could gives hint about the microscopic interpretation of the dilution in terms of reaction-diffusion kinetics of lymphocytes and their signalling (on which we plan to report soon), as, for instance, increasing the mean square velocity of these elements (e.g. via fever and increased heartbeats), decreases network dilution and, consequently, increased the quality and the strength of the signal on the B-cells.
In particular we studied in detail the case where helpers manage an amount of B-clones proportional to the logarithm of the H repertoire, so to say, if the repertoire of helpers is made of by e.g. 10^{10} different clones (like in humane immune systems), the network is able to manage at the same time $\mathcal{O}(10)$ different clonal lineage of B-cells.

This is an important step forward a rationale understanding of these lymphocyte networks because the immune system is always supposed to fight several pathogens at each time.

Turning to technicalities, we studied the model via statistical mechanics solving for the free-energy and obtaining through the extremization of the latter, the order parameter self-consistencies, which have been explicitly written for the simplest case of two and three parallel retrieved patterns. These equations have been hierarchically solved and tested against the results coming from signal-to-noise analysis and Monte Carlo simulations: Once showed that the "pure state ansatz" of neural networks in this context can no longer minimize the free energy, we introduced a "parallel ansatz" and performed the signal-to-noise analysis to confirm its validity by studying the stability of the basin of attraction of the minima it generated. Further, we performed Monte Carlo simulations to confirm numerically the whole scenario. Overall we found perfect agreement among all the results stemmed from these different techniques.

Future works, beyond the microscopical interpretation of the tunable parameters, would investigate the saturated case, which is still mathematically challenging; then the system in presence of antigens (fields) and a detailed refinement discriminating between B-clones (which here are all supposed to share the same structural characteristics) with low/high avidity against own tissues with the aim of showing further emerging properties as the clonal anergy for high avidity B-clonal lineages resulting in self/non-self discrimination problems.

Acknowledgments

AB is grateful to Guido Valesini and Rossana Scrivo for useful conversations.
This research was sponsored by the FIRB grant RBFR08EKEV.
Sapienza Università di Roma is acknowledged too for partially supporting the work.

References

[1] A. K. Abbas, A.H. Lichtman, S. Pillai, *Basic Immunology: Functions and Disorders of the Immune System*, Saunders Elsevier, Philadelphia, PA (2009).

[2] E. Agliari, A. Barra, *A Hebbian approach to complex network generation*, Europhys. Lett. **94**, 10002, (2011).

[3] E. Agliari, A. Barra, F. Camboni, *Criticality in diluted ferromagnet*, J. Stat. Mech. *P*10003, (2008).

[4] E. Agliari, A. Barra, F. Guerra, F. Moauro, *A thermodynamic perspective of immune capabilities*, J. Theor. Biol. **287**, 48-63, (2011).

[5] D.J. Amit, *Modeling Brain Function*, Cambridge University Press, UK, (1989).

[6] D.J. Amit, H. Gutfreund, H. Sompolinsky, *Information storage in neural networks with low level of activity*, Phys. Rev. A **35**, 5, 2293, (1987).

[7] D.J. Amit, H. Gutfreund, H. Sompolinsky, *Storing infinite numbers of patterns in a spin glass model of neural networks*, Phys. Rev. Lett. **55**, 3354, (1985).

[8] A. Barra, E. Agliari, *Autopoietic immune networks from a statistical mechanics perspective*, J. Stat. Mech. P07004, (2010).

[9] A. Barra, E. Agliari, *Stochastic dynamics for idiotypic immune networks*, Physica A **389**, 5903-5911, (2010).

[10] A. Barra, A. Bernacchia, E. Santucci, P. Contucci, *On the equivalence of Boltzman Machines and Hopfield Networks*, submitted to Neural Networks (2012).

[11] A. Barra, F. Guerra, *About the ergodicity in Hopfield analogical neural network*, J. Math. Phys. **49**, 125217, (2008).

[12] A. Barra, F. Guerra, G. Genovese, *The replica symmetric behavior of the analogical neural network*, J. Stat. Phys. **140**, 4, 784, (2010).

[13] W.N. Bailey, *Gauss's Theorem*, in Generalised Hypergeometric Series, Cambridge University Press, UK, (1935).

[14] Y. Bengio, *Learning Deep Architectures for Artificial Intelligence*, Machine Learning **2**, 1, 127, (2009).

[15] F.M. Burnet, *The clonal selection theory of acquired immunity*, Cambridge University Press, UK, (1959).

[16] P.A. Cazenave, *Idiotypic-anti-idiotypic regulation of antibody synthesis in rabbits*, Proc. Natl. Acad. Sc. **74**, 11, 5122-5125, (1977).

[17] A.C.C. Coolen, R. Kuehn and P. Sollich, *Theory of neural information processing systems*, Oxford University Press, UK, (2005).

[18] A.C.C. Coolen, A.J. Noest, *Selective Pattern Recall in Neural Networks by Chemical Modulation*, J. Phys. A **23**, 575-579, (1990).

[19] A.C.C. Coolen, A.J. Noest, G.B. de Vries, *Modelling Chemical Modulation of Neural Processes*, Network **4**, 101-116, (1993).

[20] L.F. Cugliandolo, M.V. Tsodyks, *Capacity of networks with correlated attractors*, J. Phys. A **27**, 741, (1994).

[21] A. Di Biasio, E. Agliari, A. Barra, R. Burioni, *Mean-field cooperativity in chemical kinetics*, to appear in Theor. Chem. Acc. (2012).

[22] E. Gardner, *Maximum Storage Capacity in Neural Networks*, Europhys. Lett. **4**, 481, (1987).

[23] A. Grakoui, S.K. Bromley, C. Sumen, M.M. Davis, A.S. Shaw, P.M. Allen, M.L. Dustin, *The immunological synapse: a molecular machine controlling T cell activation*, Science **285**, 221, (1999).

[24] 12.[10] in Gradshteyn

[25] G.E. Hinton, R. R. Salakhutdinov, *Reducing the Dimensionality of Data with Neural Networks*, Science **313**, 5786, 504-507, (2006).

[26] J.J. Hopfield, *Neural Networks and Physical Systems with Emergent Collective Computational Abilities*, Proc. Natl. Acad. Sci. USA **79**, 2554, (1982).

[27] R.A. Horton, L.A. Moran, G. Scrimegour, M. Perry, D. Rawn, *Principles of biochemistry*, Pearson Prentice Hall, USA (2006).

[28] N.K. Jerne, *Towards a network theory of the immune system*, Ann. Immunol. (Paris) **125** C, 373-389, (1974).

[29] I. Lundkvist, A. Coutinho, F. Varela, D. Holmberg *Evidence for a functional idiotypic network among natural antibodies in normal mice*, Proc. Natl. Acad. Sc. **86**, 5074-5078, (1989).

[30] D. Kitamura, *How the Immune System Recognizes Self and Nonself*, Springer-Verlag, Berlin, (2008).

[31] S. Kivity, N. Agmon-Levin, M. Blank, Y. Shoenfeld, *Infections and autoimmunity*, Trends Immunol. **30**, 409-414, (2009).

[32] A. Kosmrlj, A.K. Chakraborty, M. Kardar, and E.S. Shakhnovich, *Thymic selection of T-cell receptors as an extreme value problem*, Phys. Rev. Lett. **103**, 068103, (2009).

[33] Kurchoo et al., *Cytokines and autoimmune diseases*, Kurchoo et al. Editors, Humana Press, New Jersey, (2002).

[34] E. Jaynes, *Information theory and statistical mechanics*, Phys Rev **106**, 620-630, (1957).

[35] E. Jaynes, *Information theory and statistical mechanics. II.*, Phys Rev **108**, 171-190, (1957).

[36] C. Janeway, P. Travers, M. Walport, M. Shlomchik, *Immunobiology*, Garland Science Publishing, New York, NY, (2005).

[37] M. Mezard, G. Parisi, M. A. Virasoro, *Spin glass theory and beyond*, World Scientic, Singapore, (1987).

[38] T. Mora, A.M. Walczak, W. Bialek, C.G. Callan Jr, *Maximum entropy models for antibody diversity,* Proc. Natl. Acad. Sci. (USA) **107**, 5405-5410, (2010).

[39] G. Parisi, *Two signals from B cells control the expansion of T cells: Only one is immunologically specific*, Ann. Inst. Pasteur/Immunol. **139**, 177-185, (1988).

[40] P. Pereira, L. Forni, E.L. Larsson, M. Cooper, C. Heusser, A. Coutinho, *Autonomous activation of B and T cells in antigen free mice*, Eur. Journ. Immun., **16**, (1986).

[41] P. Pereira, E.L. Larsson, L.Forni, A. Bandeira, A. Coutinho, *Natural effector T lymphocytes in normal mice*, Proc. Natl. Acad. Sc. USA **82**, 7691-7695, (1985).

[42] A. S. Perelson, G. Weisbuch, *Immunology for physicists*, Rev. Modern Phys. **69**, 1219-1267, (1997).

[43] A. S. Perelson, *Immune network theory*, Immunol. Rev. **110**, 5336, (1989).

[44] I. Perez-Castillo, B. Wemmenhove, J.P.L. Hatchett, A.C.C. Coolen, N.S. Skantzos, T. Nikoletopoulos, *Analytic solution of attractor neural networks on scale free graphs*, J. Phys. A **37**, 8789-8799, (2004).

[45] G. Parisi, *A simple model for the immune network*, Proc. Natl. Acad. Sci. USA **87**, (1), 429-433, (1990).

[46] A.A. Sinha, M.T. Lopez, H.O DeVitt, *Autoimmune diseases: the failure of self-tolerance*, Science **248**, 1380, (1990).

[47] M.C. Sneller, J. Wang, J.K. Dale, W. Strober, L.A. Middleton, Y. Choi, *Clinical, immunologic and genetic features of an autoimmune lymphoproliferative syndrome associated with abnormal lymphocyte apoptosis*, Blood **89**, 1341-1348, (1997).

[48] H. Sompolinsky, *Neural networks with non linear synapses and a static noise*, Phys. Rev. A **34**, 2571, (1986).

[49] J. Thèze, *The Cytokine Network and Immune Functions*, Oxford University Press, Oxford, UK, (1999).

[50] C.J. Thompson, *Mathematical statistical mechanics*, Princeton University Press, USA, (1979).

[51] F.J. Varela, A. Coutinho, *Second generation immune networks*, Immunol Today **2** (5), 159, (1991).

[52] B. Wemmenhove, A.C.C. Coolen, *Finite connectivity attractor neural networks*, J. Phys. A **36**, 9617-9633, (2003).